

A Novel Element-Free Galerkin Method with Uniform Background Grid for Extremely Deformed Problems

Wen-Hwa Chen¹, Cheng-Te Chi and Ming-Hsiao Lee

Abstract: Based on an incremental formulation of element-free Galerkin method (EFGM), a highly efficient three-dimensional EFGM analysis procedure is proposed to deal with the structure with extremely large deformation. By this procedure, a fixed and uniform background grid, part of which coincides with the background cells employed in the conventional EFGM for numerical integration, is devised. The background grid is connected by uniformly distributed fictitious nodes which do not move during loading process even if extremely large deformation occurs. A deformable analysis domain, which is discretized by moving boundary nodes and interior nodes, is established for describing the deformation of the structure to be analyzed. When the structure is deformed under loadings, some fictitious nodes of the background grid outside the analysis domain may be included into the analysis domain as new interior nodes. Meanwhile, some interior nodes may be excluded from the analysis domain due to deformation. By a moving least square (MLS) approximation technique, a mapping procedure can then be developed for calculating the nodal displacements/ strains/stresses at those new interior nodes from those of the neighboring influencing boundary/interior nodes existing in the previous analysis domain. Although the interior nodes existing in the deformed structure may be different at each load increment, the distribution of the new interior nodes still remains uniform. Thus, the interpolation functions within the sub-domain can be determined by enough numbers of neighboring influencing boundary/interior nodes even under extremely large deformation.

To demonstrate the accuracy and efficiency of the new EFGM analysis procedure developed, two metal forming problems are tackled. Excellent agreement between the present computed results and those available in the literatures is drawn. The application of the present technique using uniform background grid for solving extremely deformed problems can also be extended to other meshless methods.

Keywords: Element-Free Galerkin Method (EFGM), Extreme Deformation, Back-

¹ Department of Power Mechanical Engineering, National Tsing Hua University, Hsinchu, Taiwan 30043, Republic of China. E-mail: whchen@pme.nthu.edu.tw

ground Grid, Metal Forming.

1 Introduction

Meshless methods have been widely studied in many engineering fields recently. As compared with finite element analysis, the meshless methods sometimes have more potential in practical applications, especially for analyzing three-dimensional complex structures. By the meshless methods, only nodes are adopted without using elements. In addition, it is easier to create higher-order approximation functions to enhance the accuracy of the solutions, if necessary. A variety of meshless methods have been developed in the literatures, e.g. element-free Galerkin method (EFGM) (Belytschko et al., 1994), reproducing kernel particle method (Liu et al., 1995), h-p clouds (Duarte and Oden, 1996a), node-by-node meshless method (Nagashima, 2000), meshfree poly-cell Galerkin method (Zheng et al., 2008) and meshless local Petrov-Galerkin (MLPG) method (Atluri and Zhu, 1998; Han and Atluri, 2004; Atluri, 2004; Sladek et al., 2006; Jarak and Soric, 2008) etc.. Among these methods, a series of MLPG mixed finite volume (Atluri et al., 2004), collocation (Atluri et al., 2006; Li and Atluri, 2008) and finite difference (Atluri et al., 2006) methods show their meshless advantages and efficiency in eliminating the time-consuming calculation of the second derivatives of the interpolation functions. Unlike the MLPG methods, however, the EFGM needs to construct background cells for numerical integration. Although the EFGM is not a truly meshless method, sometimes, it still shows its merits in dealing with various engineering problems (Chen and Guo, 2001; Chen and Chen, 2005; Chen and Lee, 2005).

While the meshless methods are quite versatile and have been applied to many engineering fields (Johnson and Owen, 2007; Wu et al., 2007; Liu et al., 2008; Sladek et al., 2008; Sageresan and Drathi, 2008), some issues are worthy of study further. For example, although some large deformation problems were examined by different meshless methods (Chen et al., 1996; Chen et al., 1997; Ren et al., 2002; Xiong et al., 2005; Han et al., 2005; Han et al., 2006; Liu et al., 2006; Gu et al., 2007; Rossi and Alves, 2007; Wen and Hon, 2007; Wong and Shie, 2008; Yuan et al., 2008), very little work was devoted to three-dimensional cases with extremely large deformation.

To solve these problems, the adaptive approach, which can modulate the solution accuracy of the analysis model by error estimation, may be a promising choice. Several adaptive meshless approaches are proposed in the literatures. Duarte and Oden (1996b) increased the node density in the regions requiring adaptivity and enhanced the degrees of polynomials to modify the accuracy of the approximation function. Similar concepts were adopted by Liu and Jun (1998), Haussler-Combe and Korn (1998), Nagashima (2000), Rabczuk and Belytschko (2005) and

Li and Lee (2006). Jun and Im (2000) raised the density of the background cells to improve the accuracy of numerical integration when the nodes were intensely crowded. Nevertheless, in addition to increase the computing cost, those adaptive meshless approaches are inherently insufficient for solving the problems with distorted nodal distribution due to extremely large deformation.

Based on an incremental formulation for the conventional EFGM, the objective of this work is to develop a new EFGM analysis procedure to deal with the three-dimensional problems with extremely large deformation. By this procedure, a background grid is constructed and discretized by uniformly distributed fictitious nodes, part of which coincides with the background cells adopted in the conventional EFGM for numerical integration. The deformable analysis domain which is described by the moving boundary nodes and the interior nodes for depicting the deformation of the structure is embedded in the background grid. For each load increment, those fictitious nodes of the background grid do not move with the analysis domain. As the structure is deformed, the analysis domain may include some fictitious nodes of the background grid outside the analysis domain as new interior nodes or exclude some interior nodes from the analysis domain. Those nodal displacements/strains/stresses of the new interior nodes within the analysis domain are determined from those of the neighboring influencing boundary/interior nodes within the previous analysis domain by a MLS approximation based data mapping procedure. Consequently, the proposed EFGM analysis procedure can not only guarantee the scattering of the new interior nodes enclosed by the boundary of the structure to be uniform, but also provide enough numbers of neighboring influencing boundary/interior nodes to calculate the interpolation functions required in the sub-domain.

Two metal forming problems are analyzed to display the efficiency and versatility of the method developed. The present computed results agree very well with referenced solutions and the comparison with ANSYS[®] finite element analysis program is also shown.

2 Incremental Formulation of Element-Free Galerkin Method

As displayed in Fig.1, a three-dimensional structure $\Omega^{(N)}$ enclosed by boundary $\Gamma^{(N)}$ at $C^{(N)}$ state is considered. As the deformation is extremely large, the nonlinear effects due to geometrical and material nonlinearities need to be taken into account. To describe the geometrical and material nonlinear effects appropriately, an incremental approach based on an Updated Lagrangian Formulation (Bathe, 1996) is adopted in this work.

As well-documented in literature (Chen and Yeh, 1988; Chen and Tasi, 1989),

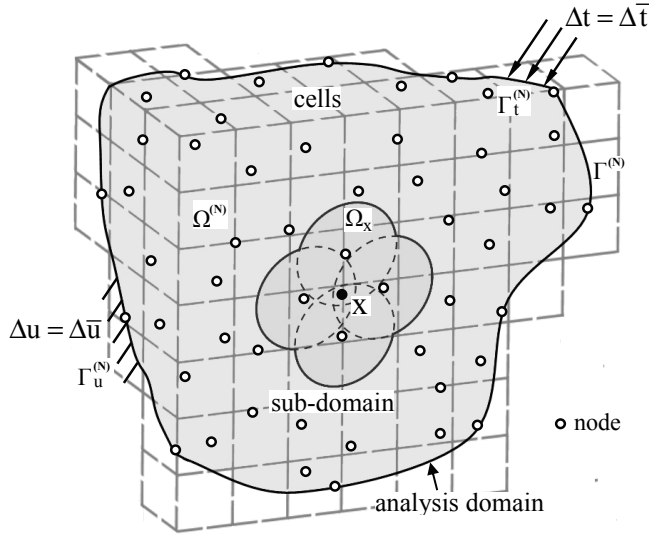


Figure 1: An incremental three-dimensional EFGM analysis model

assuming the nodal displacements, stresses and strains from $C^{(0)}$ state to $C^{(N)}$ state are already known, the incremental functional $\Delta\Pi$ from $C^{(N)}$ state to $C^{(N+1)}$ state can be formulated based on the principle of minimum total potential energy as follows (neglecting the body force term):

$$\begin{aligned} \Delta\Pi(\Delta u_i) &= \int_{\Omega^{(N)}} \left(\frac{1}{2} E_{ijkl} \Delta e_{ij} \Delta e_{kl} + \frac{1}{2} \tau_{ij}^{(N)} \Delta u_{k,i} \Delta u_{k,j} \right) d\Omega - \int_{\Gamma_t^{(N)}} \Delta \bar{t}_i \Delta u_i d\Gamma \\ &\quad - \left[\int_{\Gamma_t^{(N)}} \bar{t}_i^{(N)} \Delta u_i d\Gamma - \int_{\Gamma^{(N)}} \tau_{ij}^{(N)} \Delta e_{ij} d\Omega \right] \\ &= \min. \end{aligned} \quad (1)$$

Since the incremental displacement Δu_i from $C^{(N)}$ state to $C^{(N+1)}$ state is assumed small, the linearized incremental Green-Lagrangian strain and its corresponding incremental 2nd Piola-Kirchhoff stress can be viewed as Δe_{ij} and $E_{ijkl} \Delta e_{kl}$. E_{ijkl} represents the current constitutive property tensor. $\tau_{ij}^{(N)}$ is the Cauchy (true) stress at $C^{(N)}$ state. $\bar{t}_i^{(N)}$ and $\Delta \bar{t}_i$ are the prescribed surface traction acting on the traction boundary $\Gamma_t^{(N)}$ at $C^{(N)}$ state and its corresponding increment from $C^{(N)}$ state to $C^{(N+1)}$ state, respectively. When the material involves elasto-plastic behaviors, the von Mises yield criterion is utilized to determine whether the material point of

the structure is yielded or not. Once the material point is yielded, the elasto-plastic constitutive property tensor E_{ijkl} derived from the associated flow rule and isotropic strain hardening rule (Chen and Han, 1995) is used. The last two terms expressed in the bracket [] in Eqn. (1) serve as an equilibrium check and will vanish when $C^{(N)}$ state is in equilibrium.

By formulating the EFGM analysis procedure in matrix representation, as seen in Fig. 1, the incremental displacement vector $\{\Delta u\}$ of any point x within the analysis domain from $C^{(N)}$ state to $C^{(N+1)}$ state can be described by the incremental nodal displacement vector $\{\Delta q\}$ of neighboring nodes within the sub-domain Ω_x which will influence point x (Zhu and Atluri, 1998), say,

$$\{\Delta u\} = [\Psi] \{\Delta q\} \text{ in } \Omega_x \tag{2}$$

$[\Psi]$ is the interpolation function matrix for the incremental displacement vector $\{\Delta u\}$ within the sub-domain Ω_x . It is noted that the sub-domain Ω_x is a collection of several spherical supports of the neighboring nodes (Zhu and Atluri, 1998) which influence point x . Because there is no element connectivity in the EFGM, the incremental displacement vector $\{\Delta u\}$ of any point x is established through a moving least square (MLS) approximation (Belytschko et al., 1994) within the sub-domain Ω_x . By this MLS approximation, the established incremental displacement vector $\{\Delta u\}$ is composed of a complete monomial basis of appropriate order and an undetermined coefficient vector. The undetermined coefficient vector can be obtained by minimizing the sum of a weighted, discrete L_2 norm of the difference between the established incremental displacement vector $\{\Delta u\}$ and the incremental nodal displacement vector $\{\Delta q\}$ at each neighboring node within the sub-domain Ω_x which influences point x . The established incremental displacement vector $\{\Delta u\}$ can thus be computed and expressed in terms of the corresponding incremental nodal displacement vector $\{\Delta q\}$ of all neighboring nodes within the sub-domain Ω_x which influence point x , and the explicit form of the interpolation function matrix $[\Psi]$ in Eqn. (2) can be derived thereafter.

The linearized incremental Green-Lagrangian strain can then be derived from the incremental nodal displacement vector $\{\Delta q\}$ as

$$\{\Delta e\} = [B_L] \{\Delta q\}. \tag{3}$$

Following similar procedures as mentioned above, the derivation for the incremental displacement vector $\{\Delta u\}$ and the linearized incremental Green-Lagrangian strain of any point x within the sub-domain Ω_x can be extended to the entire analysis domain from $C^{(N)}$ state to $C^{(N+1)}$ state. Substituting Eqns. (2) and (3) into Eqn. (1) and applying the stationary condition of $\Delta \Pi$ with respect to the incremental nodal displacement vector of all the nodes within the analysis domain $\{\Delta q^*\}^T$,

say,

$$\frac{\partial \Delta \Pi}{\partial \{\Delta q^*\}^T} = \{0\}, \tag{4}$$

the incremental governing equations of the analysis domain from $C^{(N)}$ state to $C^{(N+1)}$ state can be written as

$$([K_M] + [K_G]) \{\Delta q^*\} = \{\Delta Q\} + \{\Delta Q^*\}. \tag{5}$$

In the above, $[K_M]$ and $[K_G]$ refer to the incremental stiffness matrix of the analysis domain at $C^{(N)}$ state, which account for the material nonlinearity and geometric nonlinearity due to extremely large deformation, respectively. $[K_M]$ and $[K_G]$ are defined as:

$$[K_M] = \int_{\Omega^{(N)}} [B_L]^T [E] [B_L] d\Omega, \tag{6}$$

and

$$[K_G] = \int_{\Omega^{(N)}} [B_{NL}]^T [\tau^{(N)}] [B_{NL}] d\Omega. \tag{7}$$

$[B_{NL}]$ denotes the transformation matrix derived from the incremental nonlinear strain-displacement relations and $[\tau^{(N)}]$ is the Cauchy stress matrix at $C^{(N)}$ state. Besides, $\{\Delta Q\}$ and $\{\Delta Q^*\}$ in Eqn. (5) represent the incremental external load vector from $C^{(N)}$ state to $C^{(N+1)}$ state and the equilibrium check vector at $C^{(N)}$ state, respectively, and can be shown as:

$$\{\Delta Q\} = \int_{\Gamma_t^{(N)}} [\Psi]^T \{\Delta \bar{f}\} d\Gamma, \tag{8}$$

and

$$\{\Delta Q^*\} = \int_{\Gamma_f^{(N)}} [\Psi]^T \{\bar{t}^{(N)}\} d\Gamma - \int_{\Gamma^{(N)}} [B_L]^T \{\tau^{(N)}\} d\Omega, \tag{9}$$

in which $\{\tau^{(N)}\}$ denotes the Cauchy stress vector at $C^{(N)}$ state.

To carry out the numerical integration of respective matrix in Eqn. (5) by the conventional EFGM, as shown in Fig. 1, the uniform background cells employed by Belytschko et al. (1994) for numerical integration through summing up the integral values from all the Gaussian quadrature points existing in the cells enclosed by the boundary of the analysis domain are also adopted.

3 Element-Free Galerkin Method with Uniform Background Grid

Extremely large deformation of structure may result in severely distorted element meshes in the finite element analysis. For meshless methods, the serious problem of distorted nodal distribution due to extremely large deformation still exists. To overcome this, a novel EFGM analysis procedure with uniform background grid is therefore developed herein.

The uniform background grid which coincides with the background cells used for numerical integration in the conventional EFGM analysis for the deformable analysis domain is connected by uniformly distributed fictitious nodes which remain unchanged during the loading process. By the novel EFGM analysis procedure developed, the three-dimensional initial deformable analysis domain $\Omega^{(0)}$ enclosed by its boundary $\Gamma^{(0)}$ can be discretized by the initial interior nodes and moving boundary nodes, respectively. The initial interior nodes are part of the fixed fictitious nodes scattering on the uniform background grid enclosed by the initial boundary $\Gamma^{(0)}$ at $C^{(0)}$ state. As an incremental loading from $C^{(0)}$ state to $C^{(1)}$ state is applied, for example, the moving boundary nodes discretizing the boundary $\Gamma^{(0)}$ of the initial analysis domain $\Omega^{(0)}$ may move in the background grid due to deformation and describe the deformed boundary $\Gamma^{(1)}$ of the analysis domain $\Omega^{(1)}$ accurately. When the moving boundary nodes change their locations, the region of the analysis domain $\Omega^{(1)}$ will be updated thereafter, but the updated interior nodes within the analysis domain $\Omega^{(1)}$ are still composed of relevant fixed fictitious nodes existing in the uniform background grid. Similar loading and deformation can be performed from $C^{(1)}$, $C^{(2)}$, ..., $C^{(N-1)}$ states till $C^{(N)}$ state.

As depicted in Fig. 2, while the incremental loading from $C^{(N)}$ state to $C^{(N+1)}$ state is applied, the boundary $\Gamma^{(N)}$ enclosing the deformable analysis domain $\Omega^{(N)}$ can be replaced by the updated boundary $\Gamma^{(N+1)}$ accompanying with the updated analysis domain $\Omega^{(N+1)}$. Some fictitious nodes (\bullet) in the background grid outside the analysis domain $\Omega^{(N)}$ may be included into the updated analysis domain $\Omega^{(N+1)}$ by the updated boundary $\Gamma^{(N+1)}$ as the new interior nodes (\bullet). Meanwhile, some old interior nodes (\bullet) within the analysis domain $\Omega^{(N)}$ may be excluded from the updated analysis domain $\Omega^{(N+1)}$ and become as fictitious nodes (\bullet) again. It is noted that no matter the new interior nodes included or the old interior nodes remained within the updated analysis domain $\Omega^{(N+1)}$, all coincide with the fixed fictitious nodes which distribute uniformly in the background grid.

Although the interior nodes within the deformable analysis domain to be analyzed at any state always distribute uniformly in the background grid, the interior nodes involved are different in each load increment. Hence, to determine the nodal variables at the new interior nodes accurately, a rigorous data mapping procedure is

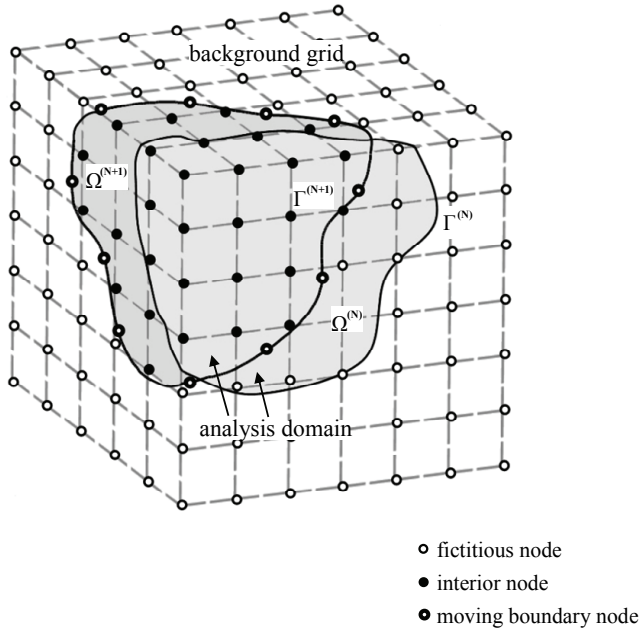


Figure 2: The novel EFGM analysis with uniform background grid

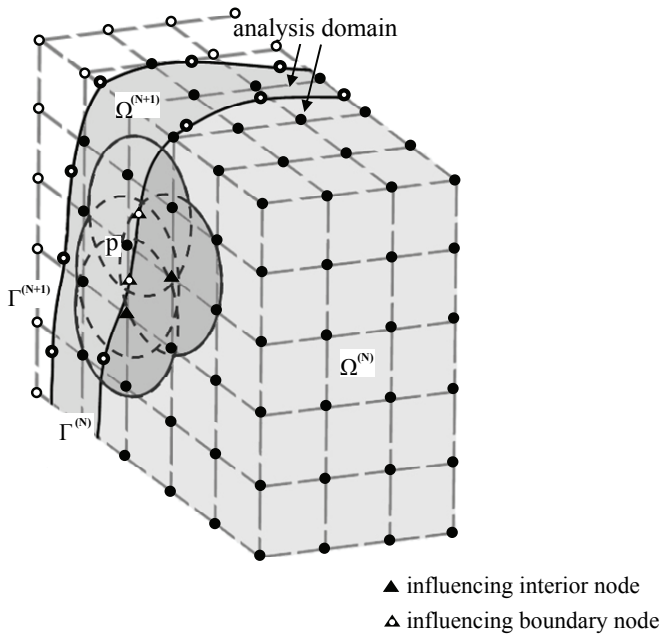


Figure 3: The scheme of data mapping

necessary. As shown in Fig. 3, assume p is a new interior node included into the analysis domain $\Omega^{(N+1)}$ from $C^{(N)}$ to $C^{(N+1)}$ state. Its sub-domain contains n spherical supports of neighboring influencing boundary nodes (Δ)/interior nodes (\blacktriangle) in the previous analysis domain $\Omega^{(N)}$, of which their nodal displacements, strains and stresses are already solved at $C^{(N)}$ state. The undetermined nodal variables of the new interior node p can thus be interpolated by those n neighboring influencing nodes within the sub-domain through the MLS approximation, as described in the above section. Similarly, the undetermined nodal variables at other new interior nodes within the analysis domain $\Omega^{(N+1)}$ from $C^{(N)}$ to $C^{(N+1)}$ state can be computed in the same way. As a result, the incremental analysis from $C^{(N)}$ state to $C^{(N+1)}$ state is achieved. It is worthwhile to mention that the size of the load increment applied and the density of the background grid taken for the analysis will affect the accuracy of data mapping. If the load increment is taken large, the updated boundary of the analysis domain for next load step may behave severe movement and result in insufficient numbers of neighboring influencing boundary/interior nodes existing in the previous analysis domain for the data mapping at some new interior nodes.

To implement the proposed EFGM analysis procedure, a uniform background grid, part of which coincides with the background cells, need be first constructed. As the analysis domain $\Omega^{(N)}$ and its boundary $\Gamma^{(N)}$ are known, for example, the fictitious nodes of the uniform background grid involved as the interior nodes for describing the analysis domain $\Omega^{(N)}$ and the moving boundary nodes discretized for the boundary $\Gamma^{(N)}$ can be determined. The incremental stiffness matrix and incremental external load vector from $C^{(N)}$ to $C^{(N+1)}$ state, as stated by Eqns. (6)–(8), are then calculated. The incremental nodal displacements and also the incremental nodal strains and stresses from $C^{(N)}$ state to $C^{(N+1)}$ state can thus be solved through Eqn. (5). Hence, the nodal variables at the interior nodes for the analysis domain $\Omega^{(N)}$ and those on the moving boundary nodes for the boundary $\Gamma^{(N)}$ from $C^{(N)}$ to $C^{(N+1)}$ state are obtained. After the nodal variables at the moving boundary nodes for the boundary $\Gamma^{(N)}$ from $C^{(N)}$ to $C^{(N+1)}$ state are solved, the deformed boundary $\Gamma^{(N+1)}$ of the updated analysis domain $\Omega^{(N+1)}$ can be defined in the background grid. For the next load step from $C^{(N+1)}$ state to $C^{(N+2)}$ state, the updated analysis domain $\Omega^{(N+1)}$ and the new interior nodes are thus determined by the boundary $\Gamma^{(N+1)}$. The data mapping procedure for the new interior nodes based on the MLS approximation is again performed accordingly. Since the incremental stiffness matrix and the equilibrium check vector expressed in Eqn. (9) are recomputed and applied for each load increment, the present solutions converge satisfactorily. The tolerance of equilibrium residual for convergence criterion is selected as 1% in this work.

As mentioned above, since the interior nodes are composed of the fictitious nodes which distribute uniformly in the background grid, the distribution quality of the interior nodes within the analysis domain at any state is guaranteed even when the structure deforms severely. In addition, sufficient numbers of neighboring influencing boundary/interior nodes are generally devoted to calculate the interpolation function matrix within the sub-domain provided appropriate size of load increment applied. Moreover, since part of the uniform background grid coincides with the background cells constructed in the analysis domain, the proposed EFGM analysis procedure not only has the inherent advantages of the conventional EFGM but also enriches its ability in dealing with the problems with extremely large deformation. Although the concept of uniform background is implemented in the EFGM analysis procedure, it can also be extended without much difficulty to other meshless methods, such as MLPG method.

4 Results and Discussions

To demonstrate the capability of the novel EFGM analysis procedure developed herein, two severely deformed metal forming problems are analyzed. The upsetting of a cylinder between two large rigid punches is first concerned. The upsetting of the same cylinder is then performed by the rigid punches having the same cross-section as that of the cylinder. The radius and length of the undeformed cylinder are 10mm and 30mm, respectively. The material of the cylinder adopted is T300 series stainless steel and its properties are known as follows: Young's modulus $E=200\text{Gpa}$, Poisson's ratio $\nu=0.3$, ultimate strength 2.14Gpa and 88% elongation at break. The bilinear isotropic hardening with yield strength $\sigma_y=0.7\text{Gpa}$ and elasto-plastic tangent modulus 0.3Gpa is found.

4.1 Upsetting by Large Punches

The first example to be solved is shown in Fig. 4. The cross-section of the rigid punches employed is much larger than that of the initial cylinder. Two frictional conditions at the interfaces are considered, respectively: one is frictionless and the other is sticking. Due to the axi-symmetry of geometry and boundary conditions, it is sufficient to deal with a small sector of the cylinder. However, to demonstrate the three-dimensional computation capability of this work, the conventional EFGM analysis model for one-eighth of the cylinder using 258 nodes is displayed in Fig.5. By contrast, the three-dimensional EFGM analysis model with the background grid at $C^{(N)}$ state in frictionless condition is illustrated in Fig.6, including 104 interior nodes and 158 moving boundary nodes. It is noted that the same number of moving boundary nodes are employed during the whole loading process, yet the number of interior nodes adopted within the cylinder may be different accompanying the

deformation of the cylinder. By applying appropriate fixed boundary conditions at the nodes in the directions perpendicular to the symmetric surfaces, a displacement control with reduction increment 4% for each load step is applied on those nodes locating at the top surface of the cylinder in both the conventional EFGM and the present novel EFGM analysis. The total reaction force P at the top surface of the cylinder can thus be calculated. Notice that the total reduction of the cylinder δ is defined as the ratio of the decrease of the length of the cylinder to the initial length of the cylinder.

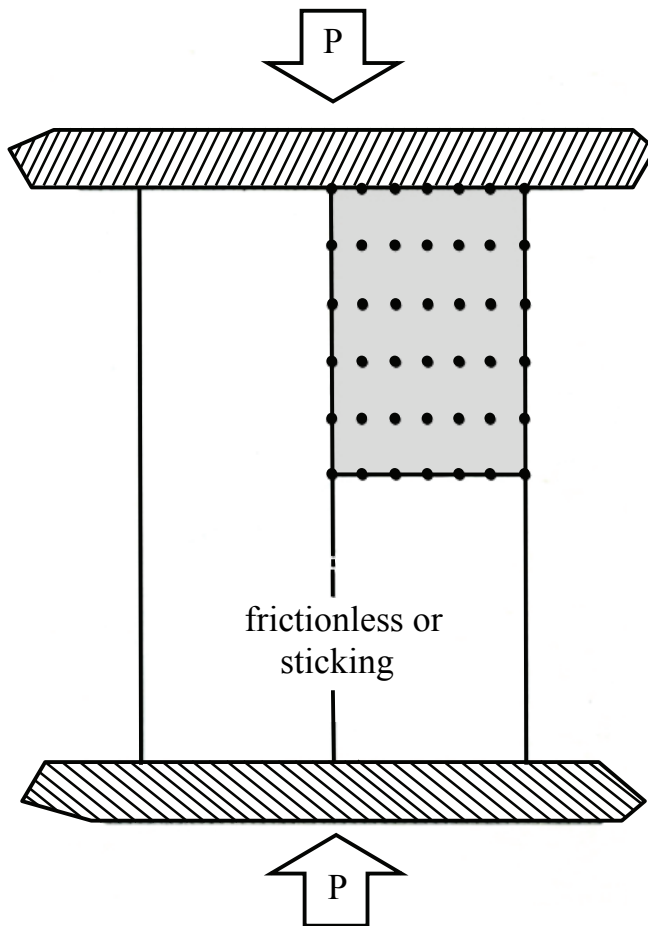


Figure 4: The upsetting of a cylinder (example I)

For the frictionless case, the nodes at the top surface of the cylinder move with the

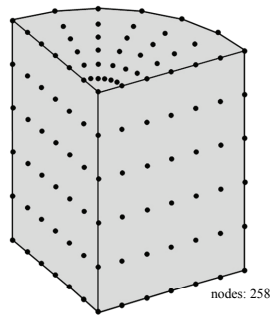


Figure 5: The three-dimensional conventional EFGM analysis model for the cylinder

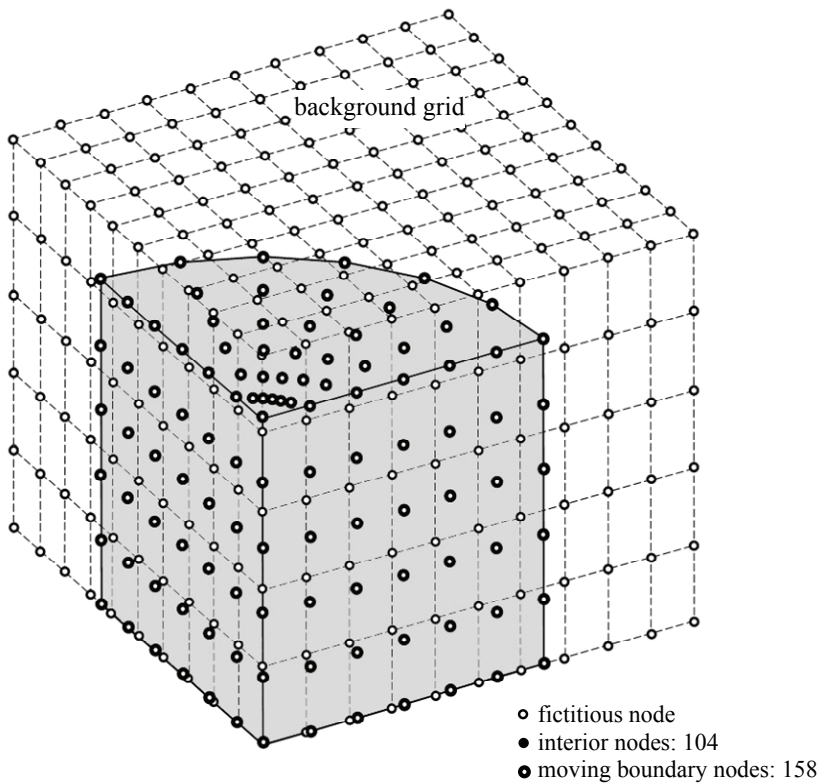


Figure 6: The three-dimensional EFGM analysis model with background grid for the cylinder (frictionless)

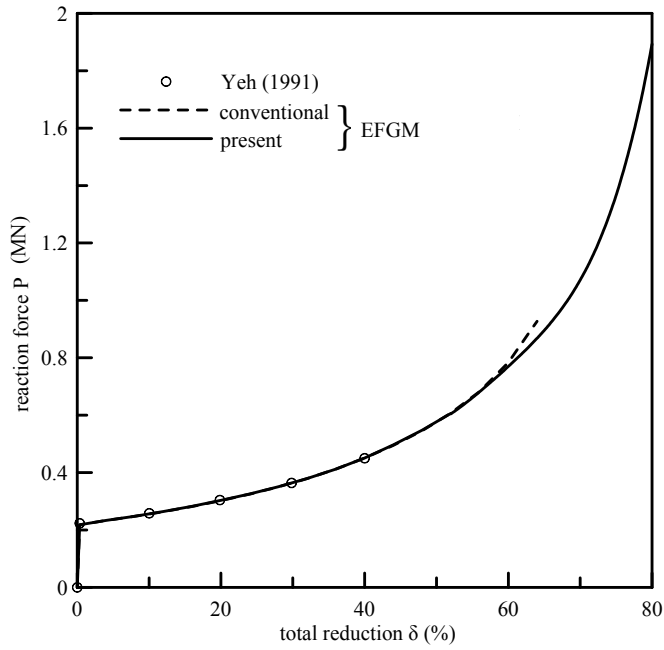


Figure 7: The reaction force vs. the total reduction (frictionless)

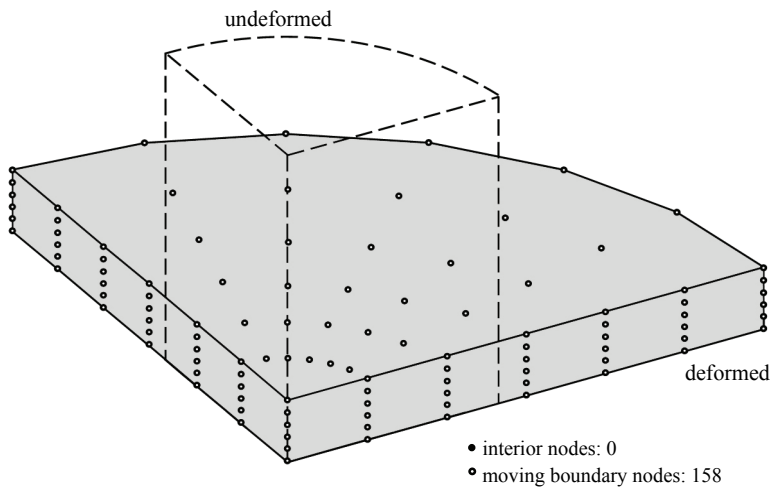


Figure 8: The deformed shape of the cylinder ($\delta=80\%$, frictionless)

rigid punch along the longitudinal direction of the cylinder, but freely slide in radial direction. The relationship between the calculated total reaction force P and the total reduction of the cylinder δ is shown in Fig.7. Both the results computed by the conventional EFGM and the present novel EFGM analysis procedures are in good agreement with the finite element solutions by Yeh (1991) using a rigorous contact mechanics analysis as the total reduction less than 40%. As the reduction continuously increases, the present novel EFGM analysis procedure still performs very well even over 80% reduction of the cylinder; however, the conventional EFGM diverges at 64% of reduction under the same tolerance of equilibrium residual taken. The deformed shape of the cylinder at 80% of reduction examined by the proposed EFGM analysis procedure is drawn in Fig.8. The maximum von Mises stress is computed as 1.18Gpa, which is under the ultimate strength 2.14Gpa. It is noted that the number of the moving boundary nodes still remains 158, but none of interior nodes within the deformed cylinder can be found. Therefore, to evaluate the deformation beyond 80% reduction of the cylinder by the present novel EFGM analysis model, sufficient number of interior nodes is imperative and the background grid adopted needs be further refined.

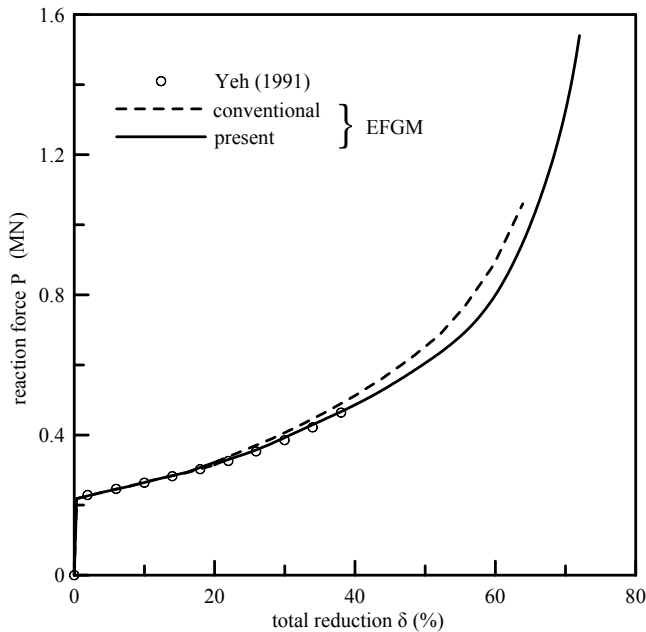


Figure 9: The reaction force vs. the total reduction (sticking)

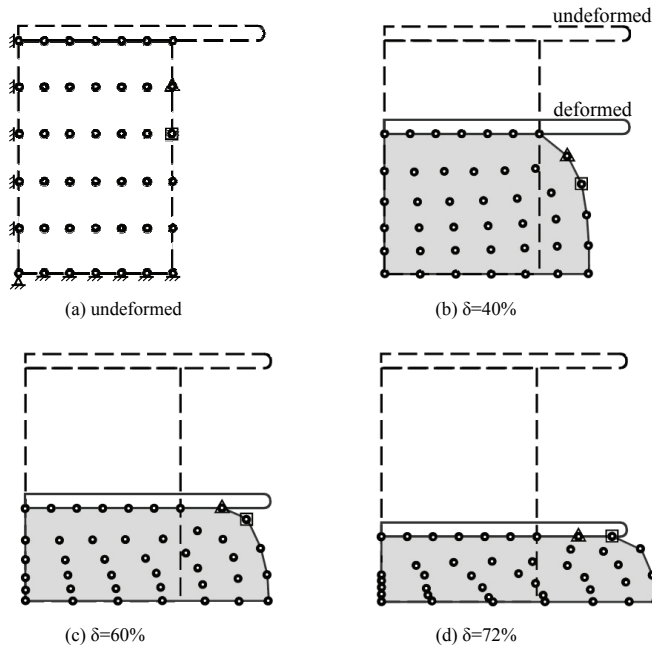


Figure 10: The deformation progress of the cylinder (sticking)

For sticking case, the nodes at the top surface of the cylinder also have the same displacements as the rigid punch in longitudinal direction of the cylinder but are completely fixed in radial direction. The relation of the computed total reaction force P versus reduction of the cylinder δ is illustrated in Fig.9. The results calculated by the novel EFGM analysis procedures are also in accordance with those by Yeh (1991) while the total reduction of the cylinder δ is smaller than 40%. However, the solutions by the conventional EFGM are stiffer than those by the present novel EFGM analysis procedure and the difference of the solutions analyzed by these two EFGM analysis models is about 5% at 40% of reduction. As the reduction of the cylinder increases further, the solutions by the conventional EFGM procedure will fail as the reduction reaches 64%, but the proposed EFGM analysis procedure still works well. The difference of the solutions calculated by these two EFGM analysis models is about 11% at 64% of reduction. The deformed progress of the cylinder affected by the sticking condition at the interface is worthy of observation. The side views of the deformation progress for a quarter of the cylinder under different reductions by the present novel EFGM analysis procedure are shown in Fig. 10, respectively. As displayed in Fig. 10, the top surface of the cylinder sticks with the rigid punch during the whole loading process. However, as the cylinder expands

in radial direction with the increase of the reduction continuously, the outer surface of the cylinder will gradually approach and attach to the bottom surface of the rigid punch, which can be demonstrated by the moving boundary nodes ▲ and ■ as shown in Fig. 10. In addition, as shown in Fig. 9, the relation between the reaction force P and the total reduction δ is expected to be stiffer after contact happens. The maximum von Mises stress occurred at the center of the deformed cylinder is about 1.46Gpa at 72% of reduction. The number of the moving boundary nodes and the interior nodes within the deformed cylinder are 158 and 90, respectively. It is noted that, although there are a few of interior nodes left within the deformed cylinder for computation, the sticking condition at the interface between the cylinder and rigid punch will cause distorted distribution for the moving boundary nodes. Since the interior nodes chosen from the uniform background grid still distribute uniformly, the computation error will be dominated by the moving boundary nodes. Hence, if the density of the background grid chosen is raised to supply more uniform interior nodes for minimizing the effect resulted from the moving boundary nodes, the calculated results can be further improved even if the reduction is beyond 72%.

4.2 Upsetting by Small Punches

In the second example, the same upsetting problem is studied except the cross-section of the rigid punches is taken as that of the undeformed cylinder with radius 10mm. The undeformed cylinder and rigid punches are displayed in Fig.11 and both frictionless and frictional ($\mu=0.3$) conditions at the interfaces between the cylinder and rigid punches are investigated. Both the conventional EFGM and the proposed novel EFGM analysis procedures are again performed with the same reduction increment 4%. To demonstrate the validity of the analyses, the results computed by ANSYS[®] finite element program, using 135 twenty-node isoparametric elements and 785 nodes, are also presented.

For frictionless case, the nodes of the cylinder at the interface between the cylinder and the rigid punches move along with the rigid punch in longitudinal direction while no constraints are provided in radial direction. Because the cross-sections of the rigid punches and the undeformed cylinder are the same, any reduction of the cylinder will result in not only the radial expansion of the cylinder, but also the separation of some nodes at the interface initially located near the edge of the cylinder. The metal flow-like warp by ANSYS[®] finite element analysis is drawn in Fig.12. Fig. 13 illustrates the relation between the total reaction force P calculated and the total reduction of the cylinder δ by various analysis models. As compared with the conventional EFGM analysis, the results evaluated by the proposed EFGM analysis procedure with background grid and ANSYS[®] finite element analysis appear to be more agreeable. However, the data calculated by the ANSYS[®] finite

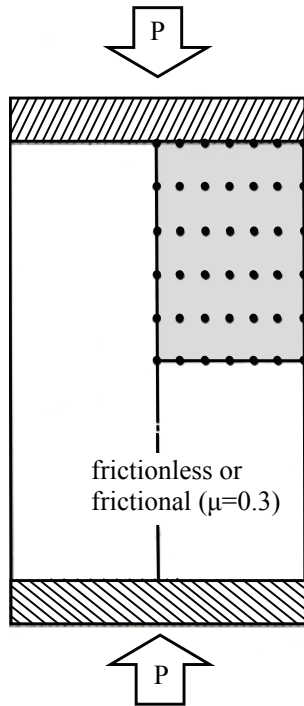


Figure 11: The upsetting of a cylinder (example II)

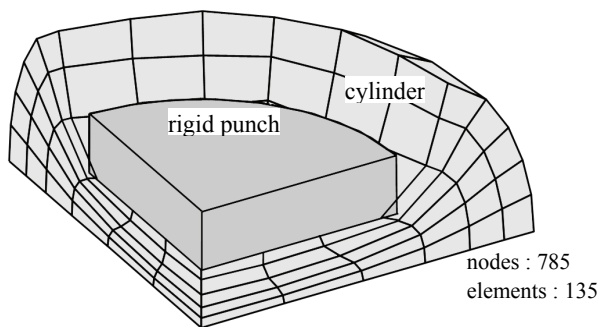


Figure 12: The deformed shape of the cylinder with $\mu=0$ by ANSYS[®] ($\delta=80\%$)

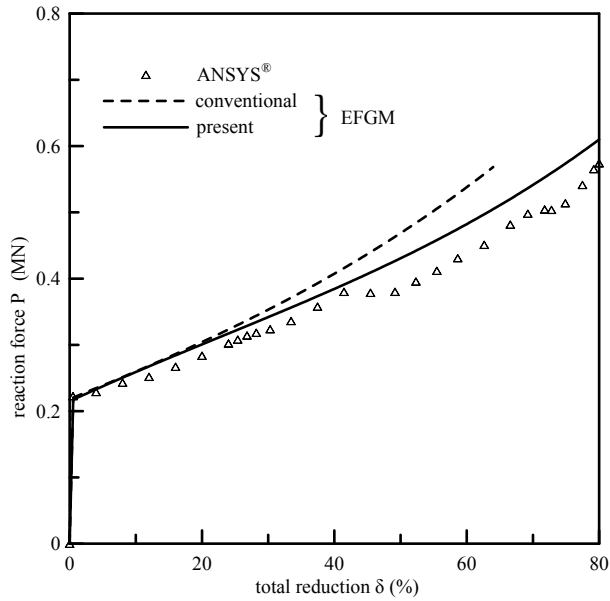


Figure 13: The reaction force vs. the total reduction ($\mu=0$)

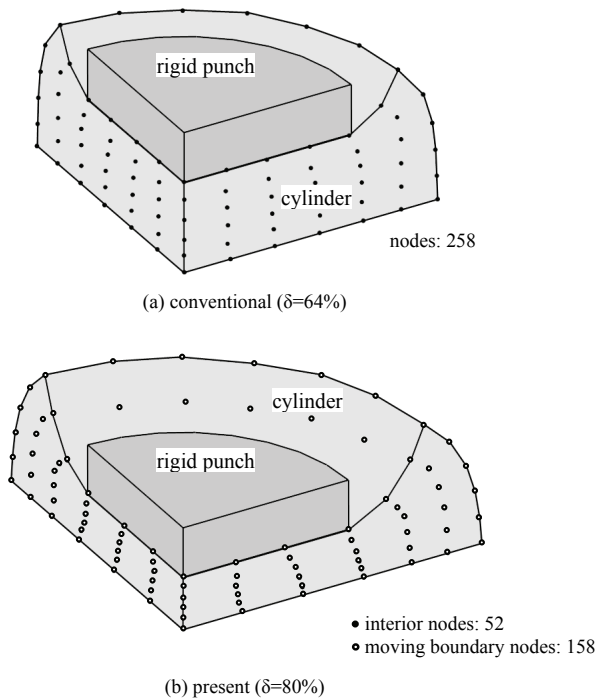


Figure 14: The deformed shapes of the cylinder by two EFGM models ($\mu=0$)

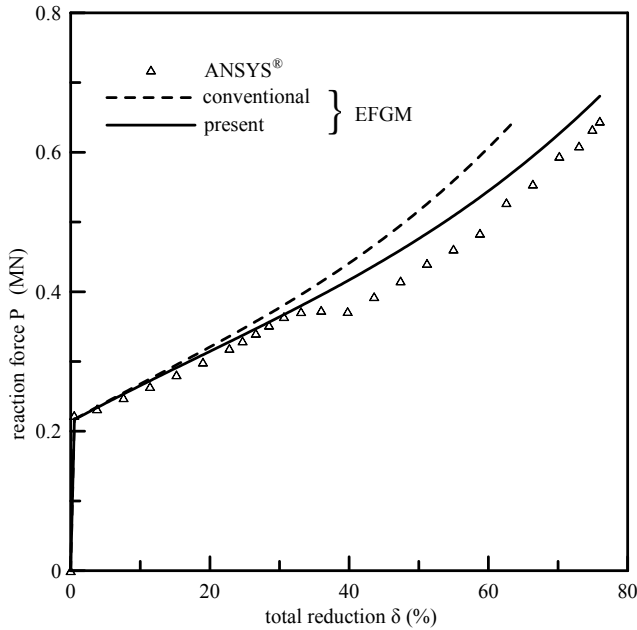


Figure 15: The reaction force vs. the total reduction ($\mu=0.3$)

element model display unreasonable fluctuations after about 40% reduction. These could be due to the unreasonable penetration of rigid punch into the top surface of the cylinder during the contact simulation, as illustrated in Fig. 12. It is worthwhile to mention that the conventional EFGM without using the background grid diverges as the reduction reaching 64% and obtains about 13% stiffer solutions. By contrast, the proposed EFGM analysis with the background grid can achieve till 80% of reduction. The deformed shapes of the cylinder at different reductions by those two EFGM analysis models are drawn in Fig.14, respectively. As observed in Fig.14, the metal flow-like warp due to longitudinal compression takes place in each model. The maximum von Mises stresses of the cylinder are found to be 1.06 Gpa and 1.24Gpa, respectively.

When the friction at the interface ($\mu=0.3$) is concerned, the movement of the nodes at the interface becomes more complicated. The nodes at the interface move in company with the rigid punches in longitudinal direction, but they can also slide in radial direction while the nodal tangential contact forces exceed their corresponding maximum static friction forces. The relationship between the total reaction force P and the total reduction of the cylinder δ by various analysis models is depicted in Fig.15. Again, as observed in Fig.15, the solution analyzed by ANSYS[®] finite

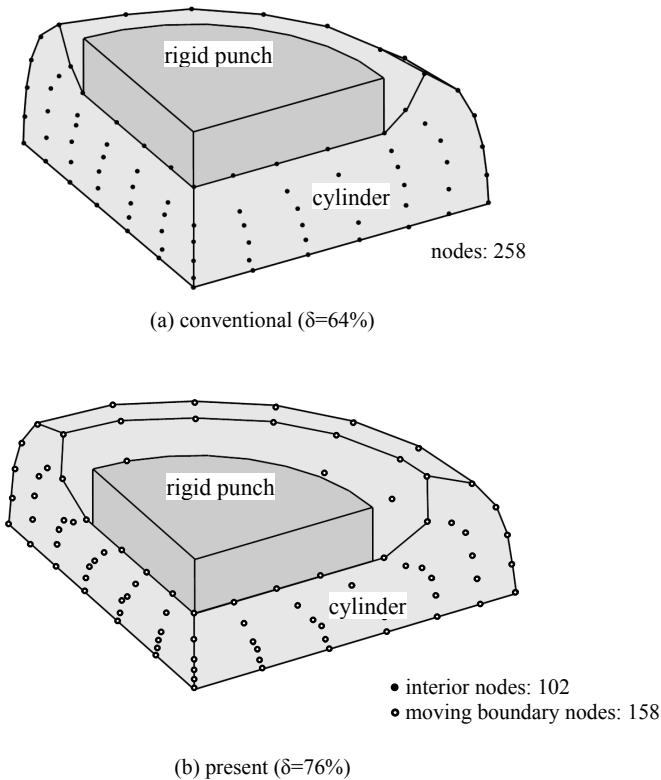


Figure 16: The deformed shapes of the cylinder by two EFGM models ($\mu=0.3$)

element model also oscillates after around 35% of reduction. Moreover, the results calculated by the present novel EFGM analysis procedure are commonly in line with those by ANSYS[®] finite element analysis but more stable. The metal flow-like warp also occurs in this case. The conventional EFGM without employing the background grid fails while the reduction after about 64%. In addition, the solution calculated by the conventional EFGM is about 12% stiffer than that by the present novel EFGM analysis procedure. The deformed shape and nodal distribution of the cylinder are displayed in Fig.16 (a) and the maximum von Mises stress is 1.19GPa. The nodal distribution of the deformed cylinder, containing 158 moving boundary nodes and 102 interior nodes, at 76% of reduction examined by the proposed EFGM analysis procedure is presented in Fig.16 (b) and the maximum von Mises stress is up to 1.34GPa.

It is noted that, although the metal flow-like warp occurs in both frictionless and frictional cases, their deformed shapes are somewhat different from each other. As

observed in Fig.16, as expected, since the radial expansion of the cylinder at the interface is resisted by the opponent friction force due to friction, the metal flow-like warp near the edge of the cylinder has a sharper slant.

5 Concluding Remarks

A novel three-dimensional EFGM analysis procedure has been successfully developed to solve the truly large deformation problems, such as severely deformed metal forming problems. The proposed EFGM analysis procedure employs a fixed and uniform background grid connecting a set of fictitious nodes. Part of the uniform background grid is overlapped with the background cells employed in the conventional EFGM for numerical integration within the analysis domain. The interior nodal distribution thus remains uniform regardless of any severe deformation. Moreover, once suitable size of load increment is selected, sufficient numbers of neighboring influencing boundary/interior nodes can be provided for calculating the interpolation functions within the sub-domain even under extremely large deformation. As compared with the conventional EFGM and ANSYS[®] finite element analyses, in addition to the intrinsic advantages of the conventional EFGM, the present proposed EFGM analysis procedure demonstrates its excellent capability in dealing with two metal forming problems solved in this work.

The method developed with a fixed and uniform background grid can also be applied to other meshless methods. However, to further explore high stress concentration problems efficiently, an adaptive scheme based on error estimation incorporated with this novel EFGM analysis procedure is imperative and will be presented in a subsequent report.

Acknowledgement: The authors would like to thank the National Science Council of the Republic of China for financially supporting this research under Contract NSC-94-2212-E-007-09.

Reference

- Atluri, S. N., Zhu, T.** (1998): A new meshless local Petrov-Galerkin (MLPG) approach in computational mechanics, *Computational Mechanics*, Vol. 22, pp. 117-127.
- Atluri, S. N.** (2004): *The Meshless Method (MLPG) for Domain & BIE Discretizations*, 680 pages, Tech Science Press.
- Atluri, S. N., Han, Z. D., Rajendran, A. M.** (2004): A New Implementation of the Meshless Finite Volume Method, Through the MLPG "Mixed" Approach, *CMES: Computer Modeling in Engineering & Sciences*, Vol. 6, no. 6, pp. 491-513.

Atluri, S. N., Liu, H. T., Han, Z. D. (2006): Meshless Local Petrov-Galerkin (MLPG) Mixed Collocation Method For Elasticity Problems, *CMES: Computer Modeling in Engineering & Sciences*, Vol. 14, no.3, pp. 141-152.

Atluri, S. N., Liu, H. T., Han, Z. D. (2006): Meshless Local Petrov-Galerkin (MLPG) Mixed Finite Difference Method for Solid Mechanics, *CMES: Computer Modeling in Engineering & Sciences*, Vol. 15, no.1, pp. 1-16.

Bathe, K. J. (1996): Finite element procedures, Prentice Hall.

Belytschko, T., Lu, Y. Y., Gu, L. (1994): Element-Free Galerkin Method, *International Journal for Numerical Methods in Engineering*, Vol. 37, pp. 229-256.

Chen, J. S., Pan, C., Wu, C.T., Liu, W.K. (1996): Reproducing Kernel Particle Methods for Large Deformation Analysis of Nonlinear Structures, *Computer Methods in Applied Mechanics and Engineering*, Vol. 139, pp. 195-227.

Chen, J. S., Pan, C., Wu, C.T. (1997): Large Deformation Analysis of Rubber Based on Reproducing Kernel Particle Methods, *Computational Mechanics*, Vol. 19, pp. 211-227.

Chen, W. H., and Yeh, J. T. (1988): Finite element analysis of finite deformation contact problems with Friction, *Computers and Structures*, Vol. 29, no. 3, pp. 423-436.

Chen, W. H., Tsai, P. (1989): Finite element analysis of an involute gear drive considering friction effects, *Journal of Engineering for industry, Transaction of the ASME*, Vol. 111, no. 1, pp. 94-100.

Chen, W. H., Guo, X. M. (2001): Element Free Galerkin Method for Three- Dimensional Structural Analysis, *CMES: Computer Modeling in Engineering & Sciences*, Vol. 2, no. 4, pp. 497-508.

Chen, W. H., Chen, C. H. (2005): On Three-Dimensional Fracture Mechanics Analysis by an Enriched Meshless Method, *CMES: Computer Modeling in Engineering & Sciences*, Vol. 8, no. 3, pp. 177-190.

Chen, W. H., Lee, M. S. (2005): On Three-Dimensional Electrostatical- structural Analysis Using Galerkin Meshless Method, *The 29th National Conference on Theoretical and Applied Mechanics*. Hsinchu, Taiwan, R.O.C., 16-17 December 2005.

Chen, W. F., Han, D. J. (1995): Plasticity for Structural Engineers, Gau Lih Book Co., Ltd.

Duarte, C. A., Oden, J. T. (1996a): H-p Clouds – An h-p Meshless Method, *Numerical Methods for Partial Differential Equations*, Vol. 12, pp. 673-705.

Duarte, C. A., Oden, J. T. (1996b): An h-p adaptive method using clouds, *Computer Methods in Applied Mechanics and Engineering*, Vol. 139, pp. 237-262.

Gu, Y.T., Wang, Q.X., Lam, K.Y. (2007): A meshless local Kriging method for large deformation analyses, *Computer Methods in Applied Mechanics and Engineering*, Vol. 196, no. 9-12, pp. 1673-1684.

Han, Z. D., Atluri, S. N. (2004): Meshless Local Petrov-Galerkin (MLPG) Approaches for Solving 3D Problems in Elasto-Statics, *CMES: Computer Modeling in Engineering & Sciences*, Vol. 6, no. 2, pp. 169-188.

Han, Z. D., Rajendran, A. M., Atluri, S. N. (2005): Meshless Local Petrov-Galerkin (MLPG) Approaches for Solving Nonlinear Problems with Large Deformations and Rotations, *CMES: Computer Modeling in Engineering & Sciences*, Vol. 10, no. 1, pp. 1-12.

Han, Z. D., Liu, H. T., Rajendran, A. M., Atluri, S. N. (2006): The Applications of Meshless Local Petrov-Galerkin (MLPG) Approaches in High-Speed Impact, Penetration and Perforation Problems, *CMES: Computer Modeling in Engineering & Sciences*, Vol. 14, no. 2, pp. 119-128.

Hussler-Combe, U., Korn, C. (1998): An adaptive approach with the element-free Galerkin method, *Computer Methods in Applied Mechanics and Engineering*, Vol. 162, pp. 203-222.

Johnson, J.N., Owen, J.M. (2007): A Meshless Local Petrov-Galerkin Method for Magnetic Diffusion in Non-magnetic Conductors, *CMES: Computer Modeling in Engineering & Sciences*, Vol. 22, no. 3, pp. 165-188.

Jarak, T., Soric, J. (2008): Analysis of rectangular square plates by the mixed Meshless Local Petrov-Galerkin (MLPG) approach, *CMES: Computer Modeling in Engineering & Sciences*, Vol. 38, no. 3, pp. 231-261.

Jun, S., Im, S. (2000): Multiple-scale meshfree adaptivity for the simulation of adiabatic shear band formation, *Computational Mechanics*, Vol. 25, pp.257-266

Li, Q., Lee, K-M. (2006): An adaptive meshless method for magnetic field computation, *IEEE Transactions on Magnetics*, Vol. 42, no. 8, pp. 1996-2003.

Li, S., Atluri, S. N. (2008): The MLPG Mixed Collocation Method for Material Orientation and Topology Optimization of Anisotropic Solids and Structures, *CMES: Computer Modeling in Engineering & Sciences*, Vol. 30, no.1, pp. 37-56.

Liu, H. T., Han, Z. D. Rajendran, A. M., Atluri, S. N. (2006): Computational Modeling of Impact Response with RD Damage Model and Meshless Local Petrov-Galerkin (MLPG) Approaches, *Computers, Materials, & Continua*, Vol. 4, no. 1, pp. 43-54.

Liu, Y. H., Chen, S. S., Li, J., Cen, Z. Z. (2008): A Meshless Local Natural Neighbour Interpolation Method Applied to Structural Dynamic Analysis, *CMES: Computer Modeling in Engineering & Sciences*, Vol. 31, no.3, pp. 145-156.

Liu, W. K., Jun, S., Zhang, Y. F. (1995): Reproduction Kernel Particle methods, *International Journal for Numerical Methods in Fluids*, Vol. 20, pp. 1081-1106.

Liu, W. K., Jun, S. (1998): Multiple-scale reproducing kernel particle methods for large deformation problems, *International Journal for Numerical Methods in Engineering*, Vol. 41, pp. 1339-1362.

Nagashima, T. (2000): Development of a CAE system based on the node-by-node meshless method, *Computer Methods in Applied Mechanics and Engineering*, Vol. 187, pp.1-34.

Rabczuk, T., Belytschko, T. (2005): Adaptivity for structured meshfree particle methods in 2D and 3D, *International Journal for Numerical Methods in Engineering*, Vol. 63, no. 11, pp. 1559-1582.

Ren, J., Liew, K.M., Meguid, S. A. (2002): Modeling and simulation of the superelastic behaviour of shape memory alloys using the element-free Galerkin method," *International Journal of Mechanical Sciences*, Vol. 44, pp. 2393-2413.

Rossi, R., Alves, M. K. (2007): On the analysis of an EFG method under large deformations and volumetric locking, *Computational Mechanics*, Vol. 39, no. 4, pp. 381-399.

Sageresan, N., Drathi, R. (2008): Crack Propagation in Concrete Using Meshless Method, *CMES: Computer Modeling in Engineering & Sciences*, Vol. 32, no.2, pp. 103-112.

Sladek, J., Sladek, V., Wen, P. H., Aliabadi, M.H. (2006): Meshless Local Petrov-Galerkin (MLPG) Method for Shear Deformable Shells Analysis, *CMES: Computer Modeling in Engineering & Sciences*, Vol. 13, no.2, pp. 103-117.

Sladek, J., Sladek, V., Tan, C.L., Atluri, S.N. (2008): Analysis of Transient Heat Conduction in 3D Anisotropic Functionally Graded Solids, by the MLPG Method, *CMES: Computer Modeling in Engineering & Sciences*, Vol. 32, no.3, pp. 161-174.

Wen, P. H., Hon, Y. C. (2007): Geometrically Nonlinear Analysis of Reissner-Mindlin Plate by Meshless Computation, *CMES: Computer Modeling in Engineering & Sciences*, Vol. 21, no.3, pp. 177-191.

Wong, S., Shie, Y. (2008): Large Deformation Analysis with Galerkin based Smoothed Particle Hydrodynamics, *CMES: Computer Modeling in Engineering & Sciences*, Vol. 36, no.2, pp. 97-117.

Wu, X. H., Shen, S. P., Tao, W. Q. (2007): Meshless Local Petrov-Galerkin Collocation Method for Two-dimensional Heat Conduction Problems, *CMES: Computer Modeling in Engineering & Sciences*, Vol. 22, no.1, pp. 65-76.

Xiong, S., Liu, W. K., Cao, J., Li, C.S., Rodrigues, J.M.C., Martins, P.A.F.

(2005): Simulation of bulk metal forming processes using the reproducing kernel particle method, *Computers and Structures*, Vol. 83, no. 8-9, pp. 574-587.

Yeh, J. T. (1991): Three-Dimensional Finite Element Analysis of Contact Problems with Friction, Ph.D thesis, Department of Power Mechanical Engineering, National Tsing Hua University.

Yuan, W., Chen, Y., Gagalowicz, A., and Liu, K. (2008): Application of Meshless Local Petrov-Galerkin (MLPG) Method in Cloth Simulation, *CMES: Computer Modeling in Engineering & Sciences*, Vol. 35, no. 2, pp. 133-154.

Zheng, C., Wu, S. C., Tang, X. H., Zhang, J. H. (2008): A meshfree poly-cell Galerkin (MPG) approach for problems of elasticity and fracture, *CMES: Computer Modeling in Engineering & Sciences*, Vol. 38, no. 2, pp. 149-178.

Zhu, T., Atluri, S. N. (1998): A Modified Collocation Method and a Penalty Formulation for Enforcing the Essential Boundary Conditions in the Element Free Galerkin Method, *Computational Mechanics*, Vol. 21, pp. 211-222.

